Electrostatic and hydrodynamics effects in a sedimented magnetorheological suspension

P. Domínguez-García,[1,*] J. M. Pastor,[2] Sonia Melle,[3] and Miguel A. Rubio[4]

[1]*Depto. Física de Materiales, UNED, Senda del Rey 9, 28040 Madrid, Spain*
[2]*Depto. Ciencia y Tec. Apl. I.T. Agrícola, E.U.I.T. Agrícolas, UPM, C. Universitaria s/n, 28040 Madrid, Spain*
[3]*Depto. Óptica, Universidad Complutense de Madrid, Arcos de Jalón s/n, 28037 Madrid, Spain*
[4]*Depto. Física Fundamental, UNED, Senda del Rey 9, 28040 Madrid, Spain*

We present experimental results on the equilibrium microstructure of a sedimented magnetorheological suspension, namely, an aqueous suspension of micron-sized superparamagnetic particles. We develop a study of the electrical interactions on the suspension by processing video-microscopy images of the sedimented particles. We calculate the pair distribution function, $g(r)$, which yields the electrostatic pair potential $u(r)$, showing an anomalous attractive interaction for distances on the order of twice the particle diameter, with characteristic parameters whose values show a dependence with the two-dimensional concentration of particles. The repulsive body of the potential is adjusted to a DLVO expression in order to calculate the Debye screening length and the effective surface charge density. Influence of confinement and variations on the Boltzmann sedimentation profile because of the electrostatic interactions appear to be essential for the interpretation of experimental results

I. INTRODUCTION

Magnetorheological [1] (MR) fluids are colloidal dispersions of micron-sized particles in a low-viscosity carrier fluid. Under the action of a magnetic external field, the particles acquire a nonpermanent dipole moment causing aggregation of particles into chainlike structures [2]. MR fluids and magnetic particles are used, by controlling the macroscopic properties, in practical applications such as electromechanical devices [3–5], biomedical laboratory techniques [6–11] and in the motion and manipulation of small fluid drops in microfluidics [12].

Controlling the formation and breakup of chains, i.e., aggregation and disaggregation processes, are important for applications using this kind of fluids. Usually, two characteristic parameters are used: the volume fraction of the dispersion, ϕ (or the corresponding surface fraction, ϕ_{2D} for quasi-two-dimensional systems) and λ, the dimensionless parameter that relates the interparticle magnetic interaction and thermal energies, defined as

$$\lambda \equiv \frac{W_m}{k_B T} = \frac{\mu_0 m^2}{16\pi a^3 k_B T}, \tag{1}$$

where μ_0 is the vacuum magnetic permeability, m the magnetic moment of the particle, a a radius of the particle, k_B the Boltzmann constant, and T the temperature.

The parameter λ may be used to define a characteristic length scale, R_1 at which the dipole-dipole interaction energy is equal to the energy of thermal fluctuations, i.e., $R_1 = 2a\lambda^{1/3}$, whereas, the volume fraction defines an initial average interparticle distance, $R_0 = 2a\phi^{-1/d}$, where d is the dimensionality of the space. If, at the time the field is switched on, $R_1 < R_0$, the aggregation process should be diffusion limited, while if $R_1 > R_0$, the aggregation process should be field driven.

Obviously, devices based on dipolar fluids work within the field driven regime. However, a thorough study of the aggregation times has not been made yet. The magnetic field aggregation time should be of the order of the time obtained by solving the problem of two identical particles aggregating under a constant uniaxial magnetic field, which is $t_{ag} \simeq 2a^2(15\lambda D)^{-1}\phi_{2D}^{-5/2}$, where D is the particle diffusion coefficient $D = k_B T/6\pi\eta a$, and η the fluid viscosity. It is particularly remarkable that in recent studies of aggregation in confined systems, Brownian dynamics simulations perfectly agree with the analytical prediction, while experimental aggregation times appear to be much longer than expected [13,14]. This is not so strange if we consider that there are several subtle physical processes that come into play when dealing with particles in a fluid that get close to other particles or the container walls. Moreover, the phenomena related to electrostatic interactions of charged colloidal particles is quite intricate and until now has not been well understood, specially when confinement is present.

For instance, surface charge at the particles [15] or the walls [16] and hydrodynamic interaction effects [17] have been shown recently to play a crucial role in the dynamics of pairs of confined charged particles. Recently, a surprising finding has been made in charged colloids, consisting on the observation of anomalous attractive interactions between equally charged particles under confinement [18–20]. These investigations have been the object of controversy [21–23]. However, the attractive well appears when a charged colloid is confined using glass surfaces and on different experimental systems, such as polystyrene (PS) spheres at water-air interfaces [24]. The explanation of this phenomena, broadly speaking, seems to be related with the nonuniformal distribution of charges on the surface of the colloidal particles and confining wall [25,26].

*pdominguez@fisfun.uned.es

In this paper, we explore two possible mechanisms that might be responsible for the large aggregation times found in a previous study [13], namely, the existence of short range repulsive electrostatic interaction and the decrease in the particle diffusion coefficient due to hydrodynamic interaction with the lower cell wall. We report on an experimental study of the equilibrium microstructure of a suspension of micronsized superparamagnetic particles in water. The particles surface is covered with carboxylic groups that create a negative surface charge when submerged in water. Moreover, the particles are denser than the surrounding fluid, hence, exhibiting sedimentation. An adequate characterization of electrostatic interactions in our system may be important to understand the magnetic field-induced aggregation results [13]. In this work, we focus on the characterization of the electrostatic properties using image analysis of freely diffusing particles.

The paper is organized as follows: Sec. II contains a brief description of the experimental setup and the procedure to obtain the pair distribution function, $g(r)$. Section III comprises the results, on the pair potential, a simple double layer model and a microrheological study. Section IV discusses the results and the conclusions are summarized in Sec. V.

II. EXPERIMENTAL METHODS

A. Experimental Setup

The MR fluids are surfactant stabilized aqueous suspensions of superparamagnetic particles, supplied by Estapor (M1–070/60). These particles are composed by a PS matrix with embedded magnetite crystals of ~ 10 nm size. The particles have a diameter of 0.97 μm and a magnetite content of 54.65 wt.%, which yields a density of 1.85 g/cm^3. The surface of the latex microspheres is functionalized with carboxylic groups. Besides, sodium dodecyl sulfate (SDS) is added to the suspension at a concentration of 1 g/l to assure redispersion of the particles upon external field switch off. We have measured the zeta potential for these suspensions using a Malvern Zetasizer Nano. For pH in the range of 6–7, we have obtained values in the range from −110 to −60 mV.

These particles have been used for experiments on aggregation under an applied external magnetic field $\vec{H}$. Then, a magnetic dipole moment is induced in the particles $\vec{m} = (4\pi/3)a^3\vec{M}$, with $\vec{M} = \chi\vec{H}$, where $\vec{M}$ is the magnetization of the particle and χ the particle magnetic susceptibility. The magnetic properties of the particles have been characterized by measuring their magnetization curve throughout a VSM magnetometer, so that accurate λ values [Eq. (1)] can be obtained. The saturation magnetization measured was 42 kA/m (23 emu/g) [13].

The MR fluid is confined in a cylindrical cell made of two horizontal quartz windows and a Teflon spacer with an inner diameter of 6.5 mm and a height of 100 μm. The confined suspension sample is placed within a surrounding thermostated chamber that keeps the temperature constant during the experiments at $T = 282$ K.

For the analysis of the movement of the particles, we use a video-microscopy setup and an ulterior image processing. The imaging system consists on a Navitar long working dis-
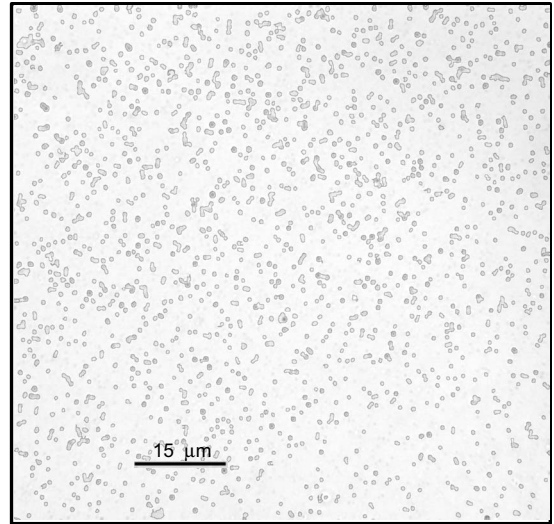

FIG. 1. Video-microscopy image showing the particles on the system.

tance microscope with zoom capabilities attached to a digital CCD camera, Retiga EX. The spatial resolution is 1360 $\times 1036$ px^2, 12 bit intensity resolution, with a maximum acquisition speed of one full frame image every 0.3 s. The image analysis has been carried out with our own developed software, based on IMAGEJ [27]. In this software, we remove the image background by thresholding and filtering and, then, we capture the contour of the clusters. In Fig. 1, we show an example of an image of the diffusing particles. Around the objects a black line can be seen marking the obtained contour.

As reported in Ref. [13], the sample cell is left 15 min without any measurement to assure that the particles have sedimented. The system of particles is quasi-2D and we focus the imaging system on the layer of particles located right above the bottom quartz window. We capture 5 min of images of freely diffusing particles without field, every 0.3 s at maximum spatial resolution, and by changing the particle surface fraction ϕ_{2D} in every experiment. The images are processed later and the position and geometrical properties of the detected objects are used to analyze the experimental data. In particular, circularity is used to discard non spherical aggregates so that isolated particles are taken into account in this study.

B. Calculation of the electrostatic potential

The sets of video-microscopy images of the sedimented particles are processed to find the particle's pair distribution function, $g(r)$, which is further processed to arrive to the expression of the DLVO electrostatic potential, allowing us to calculate the Debye screening length and the particle's effective surface charge. The pair distribution function is obtained by means of the analyzed images using the procedure described in Ref. [15]. Sequences of images are processed for each image, Then, the pair radial distribution function, $g(r)$ is obtained as
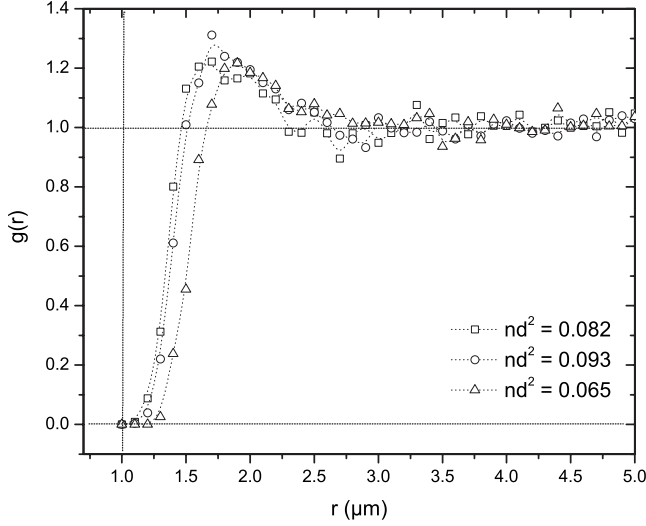
FIG. 2. Example of $g(r)$ calculated for three different experiments with $nd^2 = 0.082$, 0.093, and 0.065, where n is the number of particles per unit area and d is the particle diameter.

$$g(r) = \frac{N(r)}{\pi \delta A n^2 r}, \qquad (2)$$

where $N(r)$ is the number of pairs of particles separated a distance between r and $r + \delta$, δ is the bin width of pair distribution $N(r)$, A is the area of the region included in the snapshot, and n is the number of particles per unit area. Here, $\delta = 0.1$ μm and A is typically about 120×150 μm^2.

According to Ref. [15], it is possible to relate the number of images, N_{img}, needed to compute $g(r)$ to the measure's resolution, Δ, through

$$\Delta = \frac{A}{2\pi a \delta N_p^2 N_{img}}, \qquad (3)$$

where N_p is the number of particles in the image. In our case, $\delta = 0.1$ μm, $N_p \sim 10^3$, $A \sim 1.8 \times 10^4$ μm^2, and $a \simeq 0.5$ μm. Moreover, the images have to be statistically independent [15], so that the time interval should be larger than the particle's diffusion time $\tau = R_0^2/D$, which is $\tau \sim 20$ s. Hence, the resolution obtained with the 5 min grabbing is $\Delta \sim 10^{-2}$.

We show in Fig. 2, typical results for the obtained $g(r)$ using three independent experiments. Besides, we show in Fig. 3 an example of a pair correlation function with added salt, in this case KCl. The inclusion of salt on the suspension screens the electrostatic behavior of the particles and, consequently, we obtain a step-like function in the calculation of the $g(r)$ function.

III. RESULTS

A. Electrostatic potential results

To obtain the pair potential, we have followed again the procedure described in Ref. [15]. The $g(r)$ function is related with the interaction energy between two particles in the limit of infinite dilution by means of the Boltzmann distribution $\lim_{n \to 0} g(r) = \exp[-u(r)/k_B T]$, where n is the particle density
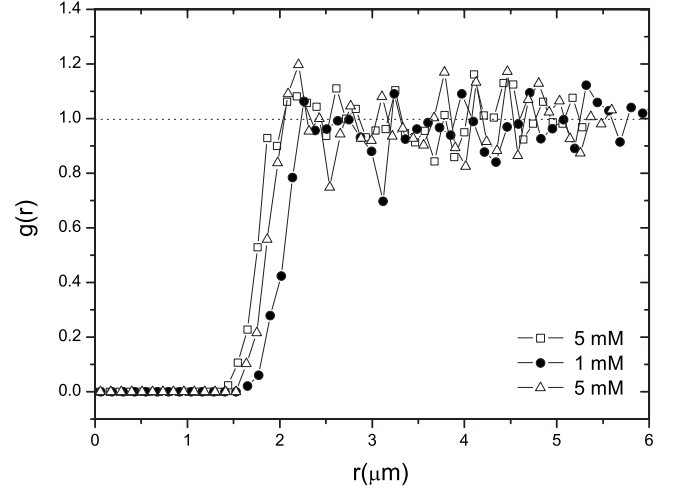

FIG. 3. Example of $g(r)$ obtained for three different experiments with added quantities of KCl in the 1–5 mM range. Electrostatic behavior has been removed by adding the salt.

and $u(r)$ the pair potential. For finite concentrations, $g(r)$ depends on the proximity of the particles, therefore, we can compute the potential of mean force $w(r) = -k_B T \ln g(r)$. No exact relationship is known between $u(r)$ and $w(r)$, but approximations can be used by means of the Ornstein-Zernike integral equation with adequate closure relations. Two popular approximations are the Percus-Yevick (PY) and the hypernetted chain (HCN). In the first case (PY), the pair potential can be calculated as

$$u(r) = w(r) + n K_B T I(r) = -k_B T[\ln g(r) - n I(r)], \qquad (4)$$

while in the hypernetted chain approximation (HCN), the pair potential is obtained as

$$u(r) = w(r) + k_B T \ln[1 + n I(r)] = -k_B T \left\{ \ln\left[\frac{g(r)}{1 + n I(r)} \right] \right\}, \qquad (5)$$

in both cases, $I(r)$ stands for the convolution integral

$$I(r) = \int [g(r') - 1 - n I(r')][g(|\mathbf{r}' - \mathbf{r}|) - 1] d^2 r', \qquad (6)$$

that is obtained by a direct iteration numerical procedure, starting from the initial condition $I(r) = 0$.

Typical results for three independent experiments are shown in Fig. 4. In all cases, the results obtained by means of the PY and HCN approximations are virtually indistinguishable, showing no difference between them in the figure. In Fig. 4 inset, we have plotted a zoom of the electrostatic potential in the proximities of $\sim 2d$. In this range a well-defined attractive well is observed with minimum values in the order of $\sim -0.2 k_B T$, a value in agreement with observations of attractive interactions of sedimented particles in confinement situation in other experimental systems [19]. The values of the potential at the minimum of the attractive well, u_{min}, and their position, r_{min}, for each experiment are summarized in Table I. In Fig. 5, we show a careful exploration of an eventual dependence of the pair potential parameters on the ex-
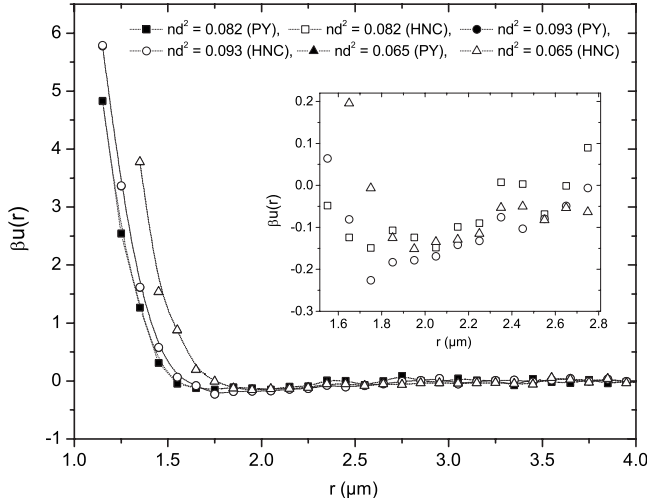
FIG. 4. Electrostatic potential $u(r)$ for three different experiments. HCN and PY approximations are indistinguishable from each other ($\beta=1/K_BT$). Inset: Detail of the range $\sim 2d$, where an attractive well is observed.

perimental parameters showing a possible dependence on ϕ_{2D}. In Fig. 5 top, the minimum values of the attractive well, u_{min}, increase when ϕ_{2D} grows; while the position of the minimum, r_{min}, decrease when ϕ_{2D} increases. Hypothesis for the explanation of this behavior are discussed later.

The short distance repulsive part of the pair potential can be casted in the form of the DLVO potential:

$$u(r) = \frac{(Z^*e)^2}{\epsilon} \frac{\exp(2a\kappa)}{(1+a\kappa)^2} \frac{\exp(-\kappa r)}{r}, \qquad (7)$$

where ϵ is the dielectric constant of the carrier fluid, κ is the inverse of the Debye screening length, and Z^* is the effective charge number of the spheres, i.e., $\sigma_{eff}=Z^*e/4\pi a^2$, where σ_{eff} stands for the effective charge density of the particles. A fit for small values of r gives an approximate value for κ and σ_{eff} for the different experiments. Table I shows the results of the fitting for each experiment.

The values obtained for charge density and Debye length are similar to those found in the case of silica particles [15]. No dependence with ϕ_{2D} is observed for the DLVO fitting-obtained values, probably because of the large dispersion. We have to point out that, in our case, the suspension is not purely two-dimensional and, hence, the video-microscopy system gets images that are 2D projections of the real 3D structure. Therefore, the distances between particles measured from the video images are generally smaller than the real 3D distances and, consequently, the pair distribution function obtained and the DLVO potential recovered shows probably a shorter range that their 3D counterparts. Average values are $\langle\kappa^{-1}\rangle=0.16\pm0.01$ μm, $\langle\sigma_{eff}\rangle=-0.10\pm0.02$ mC/m^2 and $\langle Z^*\rangle/e=1800\pm500$. Remarkably, when salt is added, the attractive region in the interparticle potential disappears, unequivocally showing that the attractive well has an electrostatic origin.

In the following sections, we discuss some possibilities to explain these results. First of all, we discuss a simple double

TABLE I. Experimental data for the attractive well values and physical magnitudes obtained by fitting the DLVO potential to the calculated electrostatic potential. Z^* is expressed in elemental charge units and $\beta=1/K_BT$. Units for σ_{eff} are mC/m^2, for κ^{-1} and $r_{min}(r)$ are μm. Calculations using PY and HCN approximations are indistinguishable. Errors are the shown in the first row.

| ϕ_{2D}	nd^2	$-\beta u_{min}(r)$	$r_{min}(r)$	Z^*	$-\sigma_{eff}$	κ^{-1}
0.031	0.018	0.14 ± 0.05	2.65 ± 0.15	3418	0.19	0.18 ± 0.02
0.038	0.020	0.12	2.54	2020	0.11	0.12
0.039	0.018	0.13	2.68	2157	0.12	0.20
0.043	0.021	0.19	2.50	4385	0.24	0.16
0.045	0.020	0.10	2.00	951	0.05	0.19
0.051	0.024	0.17	2.53	2571	0.14	0.15
0.051	0.027	0.19	2.05	1640	0.09	0.15
0.059	0.039	0.16	2.00	2229	0.12	0.11
0.068	0.030	0.20	2.12	2950	0.16	0.14
0.071	0.023	0.11	2.21	1055	0.06	0.20
0.074	0.028	0.13	2.30	1604	0.09	0.17
0.075	0.035	0.16	2.07	945	0.05	0.18
0.084	0.051	0.11	2.06	2018	0.11	0.13
0.086	0.052	0.15	1.86	1200	0.07	0.14
0.088	0.065	0.15	2.16	2986	0.16	0.13
0.106	0.050	0.06	2.16	1168	0.06	0.16
0.112	0.035	0.24	1.96	797	0.04	0.17
0.115	0.067	0.19	1.76	793	0.04	0.15
0.132	0.065	0.24	1.87	715	0.04	0.16
0.145	0.067	0.24	1.87	1057	0.06	0.13
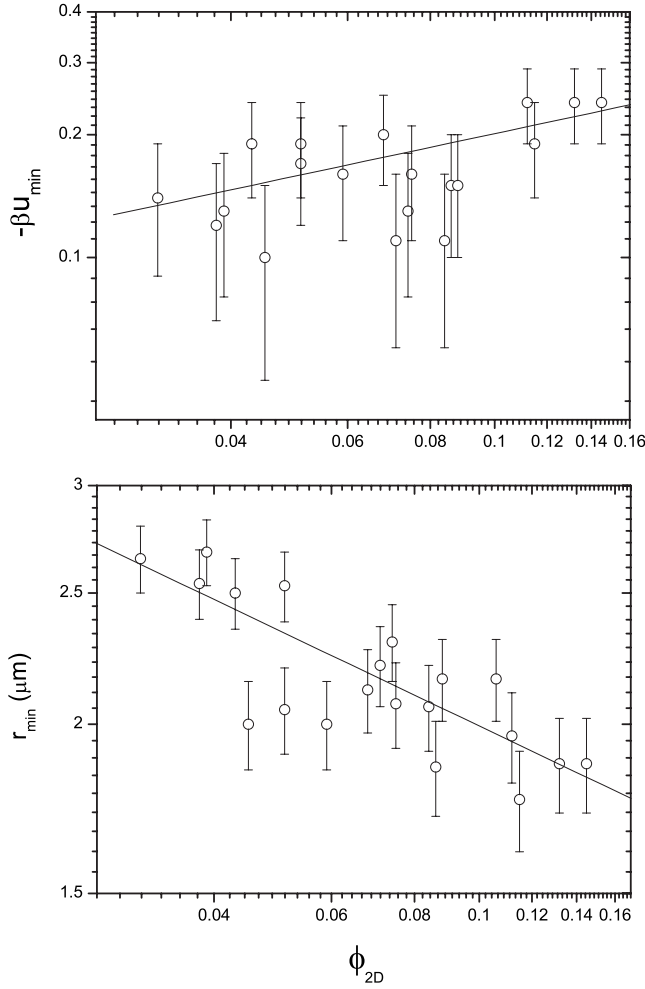
FIG. 5. Parameters of the observed attractive well as a function of the two-dimensional concentration, ϕ_{2D} (see Table I). Top: Minimum well energy, $\beta u_{\min}$. Fit: $\log(\beta u_{\min}) = (0.34 \pm 0.17) \log \phi_{2D} - (0.35 \pm 0.19)$ Bottom: Position of the minimum, $r_{\min}$ (μm). Fit: $\log r_{\min} = (-0.23 \pm 0.04) \log \phi_{2D} + (0.07 \pm 0.04)$

layer model for comparing with the measurement values for the zeta potential and the obtained values by means of the DLVO fitting.

B. Effective surface charge density

The way to compute the effective surface charge density has been thoroughly described in [16]. For the sake of completeness, we briefly reproduce here the method outlined in [16]. In our case, the surfaces of the carboxylated particles get a negative charge due to the dissociation of end groups. The carboxylic groups dissociate into −COO− groups and protons. The surface activity of protons, $[H^+]_0$, is related to the bulk activity of protons, $[H^+]_b$, and the electrostatic surface potential through the equation

$$[H^+]_0 = [H^+]_b e^{-\beta e \psi_0} \qquad (8)$$

where $[H^+]_b = 10^{-pH}$ Mol/l, and $1/\beta = K_B T$. We take the value of the dissociation constant, pK, which is $pK_p = 4.9$ for the dissociation of carboxylic groups at the particle surface [28].

Now, the basic Stern model assumes that the counterions in the solution are separated from the solid surface by a thin Stern layer of capacity C, in which the electrostatic potential drops from a value ψ_0 at the surface, to a value ψ_d. The capacity, C, relates the potential drop with the surface charge density at the solid surface, σ, i.e.,

$$C = \frac{\sigma}{\psi_0 - \psi_d} \qquad (9)$$

Experimental data suggest that an adequate range for the carboxylated polystyrene surface is $C_p > 10$ F/m^2 [16,28].

The diffuse layer potential ψ_d can be obtained as a function of the surface charge density σ by combining the equations above, together with $\sigma = -e\Gamma$ where Γ is the total surface concentration of carboxylic groups,

$$\psi_d(\sigma) = \frac{1}{\beta e} \ln\left(\frac{-\sigma}{e\Gamma + \sigma}\right) - (pH - pK)\frac{\ln 10}{\beta e} - \frac{\sigma}{C}, \quad (10)$$

where Γ can be approximated for these particles with $\Gamma = 0.25$ nm^{-2} [16].

A further relationship among the diffuse layer potential and the solid surface charge can be obtained assuming that the Poisson-Boltzmann equation holds for the distribution of mobile charges in the solution. An approximated expression for a spheric surface with radius a is

$$\sigma(\psi_d) = \frac{2\epsilon\epsilon_0 \kappa}{\beta e}\left[\sinh\left(\frac{\beta e \psi_d}{2}\right) + \frac{2}{\kappa a}\tanh\left(\frac{\beta e \psi_d}{4}\right)\right], \quad (11)$$

where $\epsilon\epsilon_0$ represents the permittivity of the solution, and κ is the inverse of the Debye screening length, namely, $\kappa^2 = n\beta e^2/\epsilon\epsilon_0$, being n the total concentration of small ions in the solution, assuming that they are monovalent.

Equations (10) and (11) can be solved self-consistently to get the values of ψ_d and σ. Those values are not experimentally accessible, however, and the values usually measured correspond to an effective surface potential, ψ_{eff}, that depends on the diffuse layer potential following the approximate expression for a surface with radius of curvature a [29]

$$\beta e \psi_{eff} = \frac{8 \tanh\left(\frac{\beta e \psi_d}{4}\right)}{1 + \left[1 - \frac{1+2\kappa a}{(1+\kappa a)^2}\tanh^2\left(\frac{\beta e \psi_d}{4}\right)\right]^{1/2}} \qquad (12)$$

Finally, the effective (measurable) charge density of the interface can be recovered from

$$\sigma_{eff} = \epsilon\epsilon_0 \kappa \psi_{eff}\left[1 + \frac{1}{\kappa a}\right] \qquad (13)$$

In Fig. 6, we plot curves corresponding to three different values of ionic strength, which yield values of the Debye length of $\kappa^{-1} = 0.10$, 0.15, and 0.20 μm, respectively. Figure 6 top shows the obtained values for the effective charge density, while Fig. 6 Bottom shows values for the effective surface potential of the particles. The lines depicted in Fig. 6 (top and bottom) represent just theoretical curves at constant values of the Debye length. In a real experiment made by adjusting the value of pH, the changes in pH will change the ionic strength, and consequently the Debye length, unless counter-ion concentration is high. The experimental value of
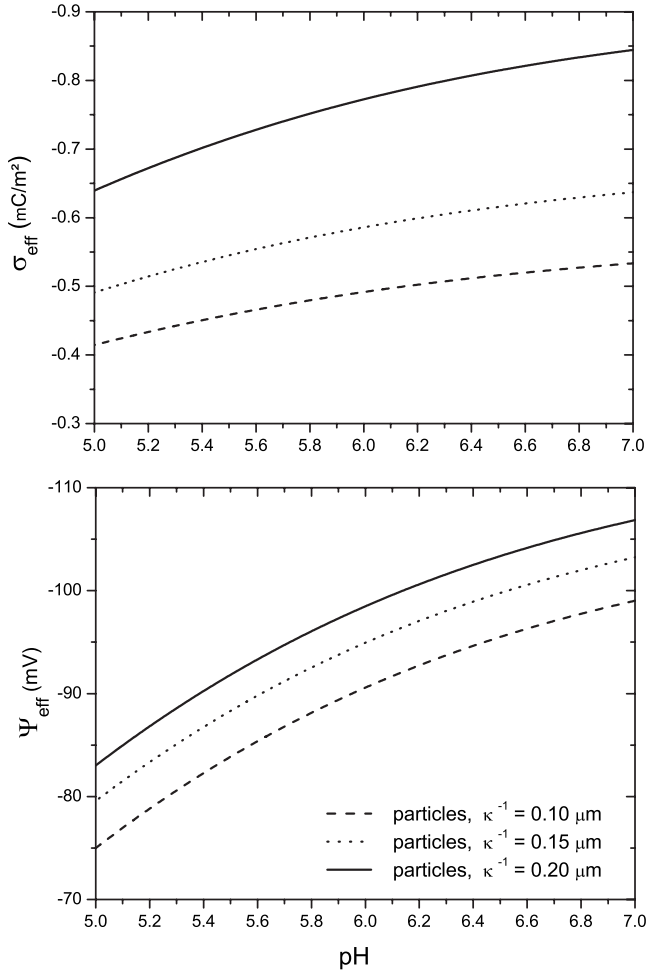
FIG. 6. Simple double layer model for the particles. Top: Effective surface charge σ_{eff} as a function of the pH for three Debye lengths. Bottom: Effective surface potential ψ_{eff}.

the suspension's pH fluctuates from one batch to another in the range $6 < pH < 7$ and the effective potential of the particles in the range $-60 < \psi_{eff} < -110$ mV. Whereas the possible values of ψ_{eff} approximately agree with the experimental values, σ_{eff} is larger than the experimental value obtained by means of the DLVO fittings. For $\kappa^{-1} \simeq 0.15$, the model predicts values in the range of -0.5 to -0.6 mC/m^2 for the absolute value of the effective charge density, and ψ_{eff} values in the range between -80 and -100 mV. While the predicted values of the surface potential are compatible with the experimental ones, the predicted and experimental values for the surface charge density show disagreement, being the experimental results five times smaller than the expected ones.

This approach can be done in a very similar way for the charging of the quartz walls due to the dissociation of silanol groups into SiO$^-$ groups and H$^+$, showing that $\sigma_{eff}^w \sim -0.2$ mC/m^2 and $\psi_{eff}^w \sim -70$ mV.

C. Microrheology of isolated particles

As mentioned before, another possible cause of a slow aggregation process might be the hydrodynamic interaction between the sedimented particles and the lower cell wall.

One way of evaluating the influence of the bottom wall in the motion of the particles is to measure the diffusion coefficient by means of microrheology techniques [30,31].

The microrheology technique here used consists on capturing images of an isolated particle at equal temporal intervals during a time lapse τ, and extracting from the images the trajectory of the particle's center of mass. Then, the Gaussian statistics of the particle displacements is obtained for each time window, and the distributions of displacements are averaged over many time windows of span τ. Finally, the width of the Gaussian statistics yields the value of the particle's diffusion coefficient.

The experimental procedure applied to the superparamagnetic particles with $d = 0.97$ μm yields a diffusion coefficient $D_{exp} = 0.23 \pm 0.01$ μm^2/s, which is significantly lower than the Stokes-Einstein prediction $(D_0 = k_B T / 6 \pi \eta a)$, which yields $D_0 = 0.343$ μm^2/s. This value of the diffusion coefficient, smaller than expected, can be explained [31] by taking into account sedimentation and hydrodynamic effects.

Particle sedimentation, that appears because of the higher density of the particle compared to the fluid density, can be treated in the following way [31]: At equilibrium, an isolated Brownian particle diffuses within the fluid, then the probability that the particle center of mass were located at a vertical position z follows a Boltzmann distribution, namely,

$$P_B(z) = \frac{e^{-z/L}}{L[e^{-a/L} - e^{(a-Z)/L}]}, \tag{14}$$

where g is the acceleration of gravity, Z is the separation between the upper and lower quartz windows, in this approximation L is the Boltzmann characteristic length $L = \frac{k_B T}{g \Delta m}$, and $\Delta m = (4/3)\pi a^3 (\rho_p - \rho_f)$, is the mass difference between the particle and a fluid volume of equal size (ρ_p and ρ_f are the densities of the particle and the fluid, respectively). Now, the average vertical position of the particle, z_g, can be calculated as

$$z_g = \frac{e^{-a/L}(aL + L^2) - e^{(a-Z)/L}[(Z-a)L + L^2]}{L[e^{-a/L} - e^{(a-Z)/L}]}, \tag{15}$$

Moreover, hydrodynamic interaction between the particle and the cell wall hinders the diffusive motion of the particle and, consequently, the diffusivity of the particle motion decreases. The corrections of the diffusion coefficients of the particle for motions parallel, $D_\parallel$, and normal, $D_\perp$ to wall are given, respectively, by

$$D_\parallel(z) = D_0 \left[1 - \frac{9}{16}\frac{a}{z} + \frac{1}{8}\left(\frac{a}{z}\right)^3 - \frac{45}{256}\left(\frac{a}{z}\right)^4 - \frac{1}{16}\left(\frac{a}{z}\right)^5 \right] \tag{16}$$

and

$$D_\perp(z) = D_0 \left\{ \frac{4}{3} \sinh \alpha \sum_{n=1}^{\infty} \frac{n(n+1)}{(2n-1)(2n+3)} \right.$$

$$\left. \times \left[\frac{2 \sinh(2n+1)\alpha + (2n+1)\sinh 2\alpha}{4 \sinh^2(n+1/2)\alpha - (2n+1)^2 \sinh^2 \alpha} - 1 \right]^{-1} \right\},$$

$$\tag{17}$$

where $\alpha = \cosh^{-1}(z/a)$, and $D_0 = k_B T/6\pi\eta a$ is the diffusion coefficient of the particle far away from the walls.

Faucheux and Libchaber [31] have shown how to properly account for the vertical diffusive motion of the particle in the computation of the effective diffusion coefficient of the particle in the direction parallel to the wall. During each time window of span τ, the particle typically explores a region of size 2δ in the vertical direction, with $\delta = \frac{1}{2}\sqrt{2\tau D_\perp}$. Then, during each time window, the particle, initially at z, will see an effective diffusion coefficient, $D_\parallel^\delta(z)$, such as

$$D_\parallel^\delta(z) = \int_{z-\delta}^{z+\delta} D_\parallel(z') P_B(z') dz'. \tag{18}$$

Assuming that the initial position z for each time window obeys the Boltzmann probability distribution and averaging over the possible initial positions one arrives at:

$$D_\parallel = \int_0^Z P_B(z) \left[\int_{z-\delta}^{z+\delta} D_\parallel(z') P_B(z') dz' \right] dz \tag{19}$$

It is important to remark, however, that z_g and, consequently, γ, depends on the particle size, a, the cell depth, Z, the difference between the densities of the particle and the carrier fluid, $\rho_p - \rho_f$, and the temperature, T. Hence, casting $D_\parallel/D_0$ as a continuous function of γ according to Fig. 4 of Ref. [31] is somewhat misleading. Actually, the predicted values reported in Table I of Ref. [31] do not belong to a single continuous curve.

We have used particles supplied by Microparticles GmbH of two types: magnetic particles and PS particles. Magnetic particles have a diameter of 8 μm with a density of 1.6 g/cm^3. These are particles with magnetic content on 45 wt.% without carboxylic groups in their surface. Their magnetic response is not very intense because of a magnetic saturation of $M_S = 20$ kA/m. The other type of particle used for testing is the PS particles of different sizes ranging from 1.1 to 9.7 μm, but all of them with a density similar to water, 1.05 g/cm^3. Two examples of calculation of diffusion coefficient of these particles can be seen on Fig. 7. We have applied the procedure exposed above to these five different sets of particles. The results are summarized in Table II.

The results exposed in Table II show good agreement between the experimental and theoretically predicted values. According to these results, the effect of sedimentation on the particles here considered is to decrease the diffusion coefficient by a factor of three in the worst case. Consequently, the hydrodynamic interaction between the sedimented particles and the lower wall of the experimental cell is not the cause of the increased aggregation times observed in this experimental system [13]. Incidentally, this decreased diffusion coefficient for strongly sedimented particles might explain the
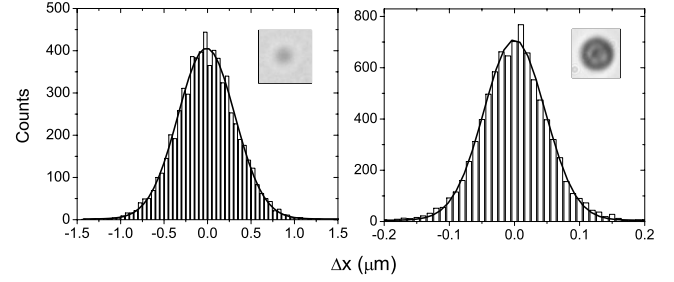

FIG. 7. Microrheology measurements for two types of particles (Inset image: example of used particles). The Gaussian fits the number of counts obtained for each Δx and gives the experimental diffusion coefficient by $D_{\exp} = w^2/8\Delta t$. Right: Magnetic particles with $d = 8$ μm, $\rho_p = 1.6$ g/cm^3 at $T = 298$ K. A Gaussian width $w = 0.093$ is obtained with a lapse between jumps of $\Delta t = 0.10$ s. and therefore $D_{\exp} = 0.011$ μm^2/s. Left: PS particles with $d = 1.1$ μm, $\rho_p = 1.05$ g/cm^3 at $T = 294$ K with $\Delta t = 0.14$ s. We obtain $w = 0.66 \pm 0.01$ and $D_{\exp} = 0.38$.

slower than expected aggregation dynamics of doublets under rotating magnetic fields [32].

IV. DISCUSSION

Here, we have studied the possible existence of electrostatic and/or hydrodynamic effects that might explain the anomalously large aggregation times found in our previous studies of magnetorheological fluids [13].

From the study of the equilibrium pair distribution function in salt-free conditions we observe an attracting region for interparticle separations in between 3 and 5 times the particle radius. The origin of this effect has to be related to an electrostatic interaction because it is not observed when we introduce high-salinity conditions into the system. Obviously, this attractive region cannot explain the increased aggregation times because its effect would be the opposite, i.e., decreasing the aggregation time. However, the potential minimum is very shallow (about $k_B T/5$), so that the effect on the aggregation time should be negligible.

The observed dependence of the values of the well depth and radial range on ϕ_{2D} in Fig. 5 may have its origin on an electrostatic repulsion with the quartz wall or because of an extended sedimentation profile resulting in an observed macroscopic electric field on charged colloids [33,34]. Small variations in the equilibrium height should affect the intensity of the anomalous attractive force, because confinement height may affect the attractive well depth and radial range values [19].

In order to explain the increased aggregation times, the repulsive part of the interparticle potential at short distances should be considered. Indeed, as shown in Fig. 4, for interparticle distances about 1.25 μm, the repulsive electrostatic potential shows values about 6 $k_B T$. At such interparticle distance, the dipole-dipole magnetic interaction energy is $U_{mag} = \lambda/(r/a)^3 \sim \lambda/2$. Hence, this repulsive part may have significant effects in the aggregation times corresponding to experiments performed at values of, say, $\lambda < 50$.

One interesting point about the Stern layer model for the charge regulation of the particle surface is that it predicts

TABLE II. Values for the theoretical equilibrium heights, z, and experimental and theoretical diffusion coefficients. Particles named PS* contain Fe_3O_4 inside them, a is the particle radius. Units: a, Z, d, L, and z_g in μm, ρ_p in g/cm^3, diffusion coefficients D_0, $D_\parallel$, and D_{exp} in μm^2/s.

Mat.	a	ρ_p	Z	T	L	z_g	D_0	D_{exp}	$D_\parallel$
PS*	0.97	1.85	100	285	0.99	1.473	0.348	0.23	0.253
PS	1.1	1.05	100	294	11.88	12.41	0.399	0.38	0.37
PS	3	1.05	100	300	0.598	2.098	0.171	0.08	0.088
PS*	8.0	1.6	100	298	0.0026	4.0026	0.061	0.011	0.019
PS	9.7	1.05	100	300	0.018	4.87	0.053	0.02	0.017

correctly the experimental values for the effective surface potential but not for the effective surface charge. One caveat is in order here: in the experiments, the surface potential and charge are measured by means of very different techniques; surface potential is measured through electrophoretic mobility techniques that use the Smoluchovski expression [29] that relates electrophoretic mobility to surface potential basically through the same approximations used in the Stern layer model. On the other hand, the experimental values of the surface charge (and the Debye length) are obtained through the fit of the experimentally obtained potential at short distances to the DLVO expression (Eq. (7)). In the present study, the results of this fit have to be taken with care, because of the small interparticle distance range available for the fit. Studies of the equilibrium pair distribution function with higher spatial resolution would be needed in order to have more accurate measurements of effective surface charge and Debye length.

However, the measured values for the effective surface charge are consistently lower than the predicted ones (approximately five times lower in average). In the framework of the Stern model, a possible cause for surface charge density values smaller than expected might be that increased values of the local proton concentration close to the particle surface (i.e., lower local values of pH) would induce proton re-association at the $-COO^-$ terminal groups. This is a consequence of the law of mass action for the reaction of dissociation of the carboxylic groups, which contributes to the second term of the right hand side of Eq. (10) (see Ref. [15], Eq. (4)). Moreover, even at short interparticle distance ($r < 2\kappa^{-1}$), below which the approximations behind the Stern model are no longer fulfilled, a more realistic formulation of the electrostatic problem [15,16] shows that below such distances the surface charge is smaller than predicted by the basic Stern model here considered. In our experiments, $2\kappa^{-1} \sim 0.3$ μm, so that this effect should not be observed, unless the Debye length is significantly underestimated. This, again, points to the need for higher resolution measurements of the equilibrium pair distribution function. Besides, and from a more general perspective, let us mention that, as stated above, local gradients in pH would induce nonuniform distributions of surface charge density. Such nonuniform distributions of surface charge density have been proposed as a possible explanation for the anomalous attractive force observed in the electrostatic potential of charged colloids [25].

Concerning the hydrodynamic interaction between the particles and the lower cell wall, the results here reported

show that the effect is at most to decrease the particle's diffusion coefficient by a factor of 3. The aggregation time between two magnetic particles under dipolar magnetic interaction is $t_{ag} \simeq 2a^2 (15\lambda D)^{-1} \phi_{2D}^{-5/2}$ [13], expression obtained from the equation of motion of the two particles. Thus, it is expected that the particles located close to the wall have an effective diffusion coefficient lower than the particles located far from the wall, so that the aggregation time for particles located close to the wall will be larger than for particles far from the wall. Consequently, since the aggregation time is proportional to D^{-1}, and we have shown that hydrodynamic interaction lowers D by a factor of three at most, this should result, at most, in an increase in the aggregation time of strongly sedimented particles by a factor of three, which is clearly less than found in [13].

Nevertheless, the combined effect of decreased diffusion and the repulsive part of the interparticle electrostatic potential at short distances might strongly affect the aggregation times up to intermediate values of, say, $\lambda < 100$. Besides, the influence of the small variations in the equilibrium height on the diffusion coefficients because of a possible extended sedimentation profile should be investigated. Numerical simulations including these effects should provide further insight on the problem. Experimental work following in detail the trajectories of two aggregating particles should also be enlightening.

V. CONCLUSIONS

We have performed experiments to determine the interparticle equilibrium interaction and particle-wall hydrodynamic interaction in sedimented magnetorheological suspensions. Experiments made through measurements of the pair distribution function show the existence of an interparticle potential of electrostatic origin with two different regions: a repulsive DLVO-like part, at short distances, and an attractive shallow well at interparticle distances between 3 and 5 particle diameters. Moreover, we have shown, through microrheology measurements, that the particle-wall hydrodynamic interaction can be explained through the combined effect of sedimentation and hindrance of diffusive particle motion close to a rigid wall. This effect amounts to a maximum threefold increase in the aggregation time under constant magnetic field. Possible ways, both through experiments and simulations, of gaining further insight into the problem have also been suggested.

[1] J. Rabinow, AIIE Trans. **67**, 1308 (1948).

[2] R. A. Kerr, Science **247**, 050401 (1990).

[3] L. Corporation (http://www.lord.com).

[4] M. Nakano and K. Koyama, in *Proceedings of the 6th International Conferences on ER and MR Fluids and their Applications* (World Scientific, Singapore, 1998).

[5] R. Tao, in *Proceedings of the 7th International Conferences on ER and MR Fluids* (World Scientific, Singapore, 2000).

[6] C. Wilhelm, F. Gazeau, and J. C. Bacri, Phys. Rev. E **67**, 061908 (2003).

[7] C. Wilhelm, J. Browaeys, A. Ponton, and J. C. Bacri, Phys. Rev. E **67**, 011504 (2003).

[8] C. Wilhelm, F. Gazeau, and J. C. Bacri, Europhys. News **36**, 89 (2005).

[9] A. K. Vuppu, A. A. García, M. A. Hayes, K. Booksh, P. E. Phelan, R. Calhoun, and S. K. Saha, J. Appl. Phys. **96**, 6831 (2004).

[10] P. Smirnov, F. Gazeau, M. Lewin, J. C. Bacri, N. Siauve, C. Vayssettes, C. A. Cuenod, and O. Clement, Magn. Reson. Med. **52**, 73 (2004).

[11] A. Komeili, Annu. Rev. Biochem. **76**, 351 (2007).

[12] A. Egatz-Gómez *et al.*, Appl. Phys. Lett. **89**, 034106 (2006).

[13] P. Domínguez-García, S. Melle, J. M. Pastor, and M. A. Rubio, Phys. Rev. E **76**, 051403 (2007).

[14] J. Cernak, G. Helgesen, and A. T. Skjeltorp, Phys. Rev. E **70**, 031504 (2004).

[15] S. H. Behrens and D. G. Grier, Phys. Rev. E **64**, 050401(R) (2001).

[16] S. H. Behrens and D. G. Grier, J. Chem. Phys. **115**, 6716 (2001).

[17] T. M. Squires and M. P. Brenner, Phys. Rev. Lett. **85**, 4976 (2000).

[18] A. E. Larsen and D. G. Grier, Nature (London) **385**, 230 (1997).

[19] Y. Han and D. G. Grier, Phys. Rev. Lett. **91**, 038302 (2003).

[20] D. G. Grier and Y. Han, J. Phys.: Condens. Matter **16**, S4145 (2004).

[21] B. V. R. Tata and N. Ise, Phys. Rev. E **58**, 2237 (1998).

[22] B. V. R. Tata and N. Ise, Phys. Rev. E **61**, 983 (2000).

[23] K. S. Schmitz, L. B. Bhuiyan, and A. K. Mukherjee, Langmuir **19**, 7160 (2003).

[24] J. S. Chen, T. Moschakis, and L. A. Pugnaloni, Food Hydrocolloids **20**, 468 (2006).

[25] Z. Lian and H. Ma, J. Phys.: Condens. Matter **20**, 035109 (2008).

[26] G. Odriozola, F. Jiménez-Ángeles, and M. Lozada-Cassou, Phys. Rev. Lett. **97**, 018102 (2006).

[27] U.S. National Institutes of Health, Bethesda, Maryland, USA (http://rsb.info.nih.gov/ij/).

[28] S. H. Behrens, D. I. Christl, R. Emmerzael, P. Schurtenberger, and M. Borkovec, Langmuir **16**, 2566 (2000).

[29] W. B. Russel, D. A. Saville, and W. R. Schowalter, *Colloidal Dispersions* (Cambridge University Press, Cambridge, England, 1989).

[30] T. G. Mason and D. A. Weitz, Phys. Rev. Lett. **74**, 1250 (1995).

[31] L. P. Faucheux and A. J. Libchaber, Phys. Rev. E **49**, 5158 (1994).

[32] P. Domínguez-García, S. Melle, O. G. Calderón, and M. A. Rubio, Colloids Surf., A **270-271**, 270 (2005).

[33] M. Rasa and A. P. Philipse, Nature (London) **429**, 857 (2004).

[34] C. P. Royall, R. van Roij, and A. van Blaaderen, J. Phys.: Condens. Matter **17**, 2315 (2005).